

RESEARCH ARTICLE

Bi-Module Sensing Device to *In Situ* Quantitatively Detect Hydrogen Peroxide Released from Migrating Tumor Cells

Ling Yu^{1,2,3*}, YunLi Tian^{1,2,3}, AnXiu Gao^{1,2,3}, ZhuanZhuan Shi^{1,2,3}, YingShuai Liu^{1,2,3*}, ChangMing Li^{1,2,3}

1 Institute for Clean energy & Advanced Materials, Faculty of Materials & Energy, Southwest University, Chongqing 400715, China, **2** Chongqing Key Laboratory for Advanced Materials and Technologies of Clean Energies, Chongqing 400715, China, **3** Chongqing Engineering Research Center for Rapid diagnosis of Fatal Diseases, Chongqing 400715, China

* lingyu12@swu.edu.cn (LY); yshliu@swu.edu.cn (YSL)



OPEN ACCESS

Citation: Yu L, Tian Y, Gao A, Shi Z, Liu Y, Li C (2015) Bi-Module Sensing Device to *In Situ* Quantitatively Detect Hydrogen Peroxide Released from Migrating Tumor Cells. PLoS ONE 10(6): e0127610. doi:10.1371/journal.pone.0127610

Academic Editor: Donghui Zhu, North Carolina A&T State University, UNITED STATES

Received: December 29, 2014

Accepted: April 17, 2015

Published: June 2, 2015

Copyright: © 2015 Yu et al. This is an open access article distributed under the terms of the [Creative Commons Attribution License](https://creativecommons.org/licenses/by/4.0/), which permits unrestricted use, distribution, and reproduction in any medium, provided the original author and source are credited.

Data Availability Statement: All relevant data are within the paper and its Supporting Information files.

Funding: This work is financially supported by Chongqing Key Laboratory for Advanced Materials and Technologies of Clean Energies, Start-up grant under SWU111071 from Southwest University, the National Science Foundation of China (No. 31200700,21375108), and Chongqing Key Natural Science Foundation (cstc2014jcyjA10070). The funders had no role in study design, data collection and analysis, decision to publish, or preparation of the manuscript.

Abstract

Cell migration is one of the key cell functions in physiological and pathological processes, especially in tumor metastasis. However, it is not feasible to monitor the important biochemical molecules produced during cell migrations *in situ* by conventional cell migration assays. Herein, for the first time a device containing both electrochemical sensing and trans-well cell migration modules was fabricated to sensitively quantify biochemical molecules released from the cell migration process *in situ*. The fully assembled device with a multi-wall carbon nanotube/graphene/MnO₂ nanocomposite functionalized electrode was able to successfully characterize hydrogen peroxide (H₂O₂) production from melanoma A375 cells, larynx carcinoma HEP-2 cells and liver cancer Hep G2 under serum established chemotaxis. The maximum concentration of H₂O₂ produced from A375, HEP-2 and Hep G2 in chemotaxis was 130±1.3 nM, 70±0.7 nM and 63±0.7 nM, respectively. While the time required reaching the summit of H₂O₂ production was 3.0, 4.0 and 1.5 h for A375, HEP-2 and Hep G2, respectively. By staining the polycarbonate micropore membrane disassembled from the device, we found that the average migration rate of the A375, HEP-2 and Hep G2 cells were 98±6%, 38±4% and 32 ±3%, respectively. The novel bi-module cell migration platform enables *in situ* investigation of cell secretion and cell function simultaneously, highlighting its potential for characterizing cell motility through monitoring H₂O₂ production on rare samples and for identifying underlying mechanisms of cell migration.

Introduction

Cell migration plays a role in many physiological and pathological processes, including tumor metastasis. [1–3] It is a physical and chemical multistep cycle including extension of a protrusion, formation of stable attachments near the leading edge of the protrusion, translocation of the cell body forward, and release of adhesions and retraction at the cell rear. [4–6] Cell

Competing Interests: The authors have declared that no competing interests exist.

migration is a prerequisite step for tumor cell invasion and metastasis that is among the most complicated and major pathologic process responsible for metastasis and poor prognosis of cancer patients.[7–9] Based on a western-blot assay, activation of multiple signalling pathways, such as extracellular signal-regulated kinase (ERK), integrin and focal adhesion kinase (FAK), are associated with cell migration.[5, 10–14] Recently, studies have shown that reactive oxygen species (ROS), particularly hydrogen peroxide (H_2O_2), diffusing freely through cellular membranes, can function as a signal messenger delivering information between signalling pathways and can even facilitate communication between cells.[15–23] Usatyuk *et al.* reported that ROS generation is responsible for hepatocyte growth factor (HGF) activated c-Met/PI3K/AKT signalling, which is an important pathway linked to cell migration.[16] Other cellular factors like Arp2/3 complex and FAK required for cell migration are also under the control of ROS.[11, 16, 17, 24] Apart from activation of signalling proteins, the influence of H_2O_2 on cell migration has been investigated through characterization of cell migration capability under exogenous H_2O_2 simulation.[21, 22, 25–27] Polyarchou *et al.* reported that exogenous H_2O_2 at a concentration of 5 μM induced human prostate adenocarcinoma LNCaP cell migration in a micro-chemotaxis chamber assay.[21] Luanpitong *et al.* evaluated the impact of various known inhibitors and donors of ROS on cell migration. Their results demonstrated that H_2O_2 (100 μM) inhibited lung carcinoma H460 cell migration and invasion in a wound healing assay.[22] This contradiction in results obtained from these studies may be rooted on the dosage of exogenous H_2O_2 , production site, as well as the tissue type of cells. The next concern is that extremely high, non-physiological concentrations of H_2O_2 were used, barely mimicking living cell environment. More importantly is that little is known about endogenous H_2O_2 levels during cell migration. In addition, from a methodology point of view, the dominant technique for characterization of cellular ROS is based on probe-labelling assays. Fluorescent histochemistry[28], flow cytometry[29] and spectrofluorimetric analysis[30] are the most widely used approaches to characterize ROS by using fluorescent dyes 2',7'-dichlorofluorescein diacetate (DCFH-DA), hydroethidine (HE) and dihydrorhodamine 123 (DHR) *etc.* These probe-labelling approaches are based on indirect methods that have been shown to be time consuming, difficult to automate and highly prone to interferences.[31] Most importantly, it is not feasible to conduct measurements *in situ* that can provide cell metabolism information and it is not feasible for characterization of cell morphology, not to mention biological functions, such as migration.[32] On the other hand, wound healing assays, trans-well assays or Boyden chamber assays, are widely used for cell migration experiments; however, they are used solely to characterize cell motility by quantifying the number of migrated cells, lacking the capability to probe biochemical changes during migration. Apart from investigation of the impact of exogenous H_2O_2 on cell migration, less attention has been paid to directly address H_2O_2 production during cell migration or invasion. Therefore, the aim of this study is to define a rational strategy enabling *in situ* monitoring of biochemical changes during the cell migration process for delineating the underlying molecular mechanisms.

Electrochemical sensors demonstrate their potential to analyse cell-secreted biomolecules.[33–36] Dr. McConnell and co-worker investigated extracellular menadiol redox activity by means of an extracellular solution containing the ferricyanide/ferrocyanide couple and a gold electrode.[37] Cytosensor microphysiometer was modified for the electrochemical detection of extracellular acidification, oxygen consumption rates or insulin.[38–40] In our previous study, as low as a 40 μL sample volume was required to probe H_2O_2 secreted from tumor cells.[41] The use of a small volume sample allows expensive reagents, particularly for rare clinical biopsies, to be conserved and makes using this analysis more cost-effective. On the other hand, the progress in lab-on-a-chip technology facilitates the study of cellular behaviour under tightly controlled microenvironments with high spatiotemporal resolution.[42–47] Previous

endeavours have focused on establishing a microenvironment that mimics *in vivo* conditions for cell migration and analysis of migration at a single cell level.[9, 42–44] But, those achievements mainly illustrated the morphology and functional changes of cells during cell migration. No studies have been reported to study biochemical molecule generation during the cell migration process.

In this work, an electrochemical sensor embedded poly(dimethylsiloxane) (PDMS) device was developed to monitor H_2O_2 *in situ* during tumor cell migration process. To achieve this goal, a multi-wall carbon nanotube (MWCNT)/graphene/ MnO_2 composite functionalized indium tin oxide (ITO) glass electrode was fabricated as a H_2O_2 sensing module. This H_2O_2 sensing module was assembled with a cell migration module that is a PDMS chamber/polycarbonate membrane/PDMS chamber sandwich structure. The fully assembled bi-module device *in situ* sensed H_2O_2 production of human melanoma cell migration under a serum established chemotaxis field. The effect of the cell H_2O_2 production inhibitor, diphenyleneiodonium (DPI), and H_2O_2 decomposition enzyme, catalase, on cell migration was also investigated on assembled devices. H_2O_2 generation and migration capability measured with assembled devices were interpreted with standard Boyden transwell assays and the results confirmed that the fully assembled bi-module device could indeed monitor H_2O_2 *in situ* during cell migration.

Materials and Methods

Materials

Graphite, multi-walled carbon nanotubes (MWCNT), ascorbic acid, 30% hydrogen peroxide, potassium hexacyanoferrate (III) ($K_3[Fe(CN)_6]$), Nafion were purchased from Aladdin, China. Phosphate buffered saline (PBS), potassium permanganate ($KMnO_4$) were from Chongqing co. Indium tin oxide (ITO) glass and silver paste were obtained from Jieshen Electronics Technology CO. Ltd (China). Printed circuit board (PCB) UV photosensitive dry film (40 μm) was obtained from IC Machinery Equipment Group (China). Human melanoma cells, A375, were obtained from ATCC. Human liver carcinoma cell line Hep G2 and human Larynx carcinoma cell line HEP-2, gifts from Dr. Yuan Li (Chongqing Medical University), were originally purchased from China Center for Type Culture Collection. The cells were maintained in RPMI 1640 medium (Gibco) with 10% fetal bovine serum (Gibco), 100 $\mu g mL^{-1}$ penicillin and 100 $\mu g mL^{-1}$ streptomycin. Phorbol 12-myristate-13-acetate (PMA), di-phenyleneiodonium (DPI), catalase and Whatman Cyclopore polycarbonate membrane (cyclopore PC circles, 5.0 μm) were purchased from Sigma Aldrich. PMA and DPI were dissolved with dimethyl sulfoxide (DMSO) to a concentration of 5 $mg mL^{-1}$ and 10 mM, respectively, as a stock solution. All other chemicals used in this study were analytical grade. The deionized (DI) water used in all experiments was produced by a Q-Grad1 system, Millipore Corporation.

Bi-module device design and fabrication

As depicted in [Fig 1A](#), the device consists of two modules: an electrochemical sensor for H_2O_2 detection and a micro trans-well platform for cell migration. From bottom to top, there are an electrochemical sensor, a PDMS chamber, a polycarbonate micropore membrane and another PDMS chamber. The micropores on the polycarbonate membrane are the channel for cells to transport from the upper chamber to the bottom chamber. [Fig 1B](#) describes the schematic diagram of the micro-fabrication process for the bi-module device. A two-electrode system was chosen to build the electrochemical sensor. The size of the working electrode and reference/counter electrode is 4.91 mm^2 and 12.8 mm^2 , respectively. To fabricate electrodes using ITO glass, a dry photosensitive film (40 μm) was coated on the ITO glass and patterned following a

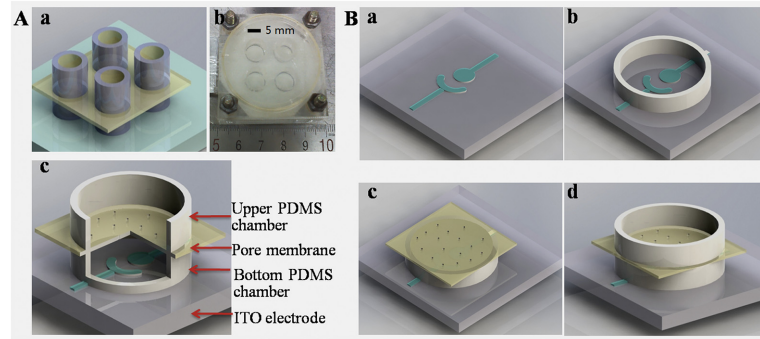


Fig 1. (A) 3D image of the bi-module device that consists of an electrochemical detection module and cell migration module (a); photograph of a device for experiment (b); section view of a bi-module device (c); (B) Schematic diagram of the micro-fabrication processes: patterning and fabrication of electrodes on a ITO glass (a); bonding of a PDMS ring (5 mm in diameter, 1 mm in height) with ITO glass (b); assembly of a polycarbonate membrane on top of the PDMS ring (c); assembly of a PDMS ring (5 mm in diameter, 5 mm in height) on top of the membrane (d). ITO: indium tin oxide, PDMS: Poly(dimethylsiloxane).

doi:10.1371/journal.pone.0127610.g001

UV photolithography process. ITO layer that was not covered by photosensitive film was dissolved by immersing the chips in etchant solution ($37\% \text{HCl} : \text{H}_2\text{O} : \text{FeCl}_3 \cdot 6\text{H}_2\text{O} = 3\text{L} : 1\text{L} : 25\text{g}$) for 30min. Finally, the patterned electrodes were recovered by removing the residue photosensitive film (a). A PDMS ring with a diameter of 5 mm and a height of 1mm was treated by plasma cleaner (Harrick, PDC-002) for 60 second and then bonded with ITO electrodes (b). To assemble a transwell chamber for assaying cell migration, a polycarbonate membrane was placed on top of the PDMS ring (c). Finally, another PDMS ring with a diameter of 5 mm and height of 5 mm was assembled on top of the polycarbonate membrane (d).

Electrochemical device for hydrogen peroxide analysis

The sensing material for hydrogen peroxide (H_2O_2) detection used in this study was a MWCNT/graphene/ MnO_2 aerogel. This functional material was synthesized according to our previous study.[41] In brief, a mixture containing MWCNT (1mg mL^{-1}), graphene oxide (1mg mL^{-1}) and KMnO_4 (10mg mL^{-1}) was prepared and stirred at room temperature for 16 h. Then, the reaction mixture was centrifuged to collect the precipitate. Next, the re-suspended precipitate was mixed with ascorbic acids solution (100 mg mL^{-1}) at 50°C for 15h to form a MWCNT/graphene/ MnO_2 hydrogel, and then freeze-dried for 24 h to completely remove water. The obtained aerogel (MWCNT/graphene/ MnO_2) was dispersed in $500\text{ }\mu\text{L}$ of ethanol (5 mg/mL) and casted onto the surface of ITO working electrodes. The MWCNT/graphene/ MnO_2 -functionalized electrode was characterized by cyclic voltammetry (CV) in 0.5 M KCl solution containing $50\text{ mM K}_3\text{Fe}(\text{CN})_6$ at the scan rate of 10 mVs^{-1} . Then the amperometric response of the fully assembled electrochemical sensor to H_2O_2 was characterized with RPMI 1640 medium according to the literature.[41] To analyse the stability of the MWCNT/graphene/ MnO_2 functionalized electrode, the electrode was immersed in the cell culture medium for 24 h. The CV response of the electrode was recorded when adding H_2O_2 ($4\text{ }\mu\text{M}$) in to the cell culture medium at 0, 12, 18 and 24 h and the changes of reduction peak current of the CV curve was compared.

Quantification of H_2O_2 production from migrating cell in a fully assembled device

Human melanoma A375 cells, liver cancer Hep G2 and larynx carcinoma HEP-2 cells were cultured in RPMI 1640 medium supplemented with 10% FCS under standard conditions (37°C , 5%

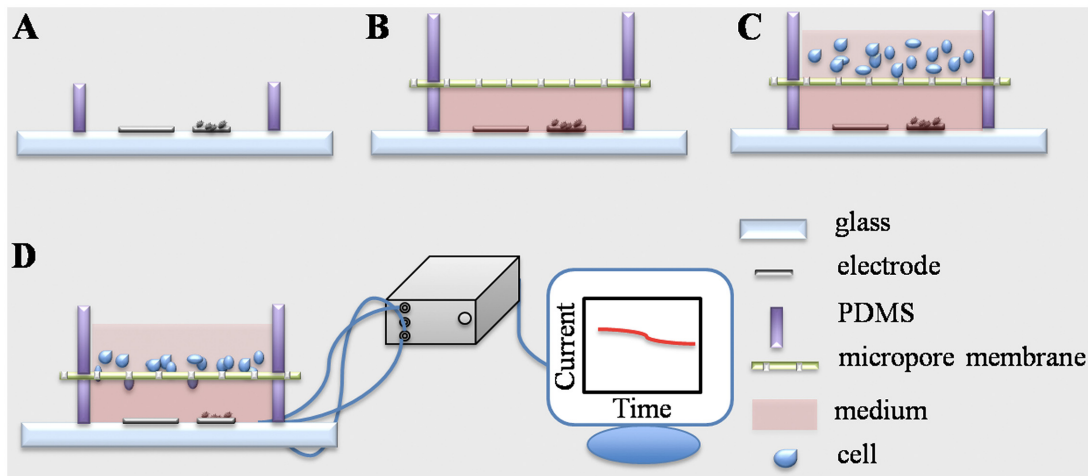


Fig 2. Experimental protocol for the electrochemical detection of H_2O_2 production during cell migration. (a) MWCNT/graphene/ MnO_2 functional material is casted on working electrode (right one) surface following a layer of Nafion coating; (b) RPMI 1640 medium is injected into the PDMS ring (bottom) using a micropipette; then polycarbonate membrane is placed on top of the PDMS ring (bottom), and another piece of PDMS ring (upper) is aligned over the membrane; (c) cell suspension is injected into the upper cell seeding chamber using a micropipette; (d) the cell-loaded device is incubated in a cell incubator for 12h and the electrochemical signal is recorded. MWCNT: mutil-wall carbon nanotube, PDMS: Poly(dimethylsiloxane).

doi:10.1371/journal.pone.0127610.g002

CO_2). Fig 2 illustrates the measurement settings. A functional sensing material, MWCNT/graphene/ MnO_2 in ethanol (5 mg/mL), was cast on the working electrode. Then one microliter of Nafion that was diluted in ethanol (1:30, V/V) was casted (a). 50 μ L of RPMI 1640 medium, with or without serum, was placed in the bottom PDMS chamber. A polycarbonate membrane and another PDMS ring were assembled on top of the bottom chamber in order (b). Next, serum-starved tumor cells (1×10^6) in 100 μ L serum-free RPMI 1640 medium were placed into the top chamber (c). All steps were conducted in a biological hood with caution to avoid microorganism contamination. Finally, the device with cell-loading was placed in a cell culture incubator maintaining stable temperature and CO_2 atmosphere (37°C, 5% CO_2). The copper wires were linked to an electrochemical station (CHI 760) and the amperometric signal (*i-t* curve) was recorded for 12 h (d). The signal from the device without cell loading was recorded as a basal control. Cells incubated with a H_2O_2 generation inhibitor DPI (10 μ M) and a H_2O_2 decomposer catalase (5 μ g mL^{-1}) were measured in parallel. Since the DPI and PMA were dissolved in DMSO, the impact of this organic solvent (0.5%, V/V) on H_2O_2 production was evaluated. After electrochemical measurement, the polycarbonate membrane in the device was disassembled and the migrated cells were visualized by hematoxylin and eosin (H&E) staining. In brief, the membrane was immersed in 4% paraformaldehyde solution for 10 min and then stained by hematoxylin and eosin solution for 10 and 2 min, respectively. Finally, loosely attached cells on topside of the membrane were removed by scrubbing twice with cotton tipped swab.[48] The cell visualized on the bottom side of the membrane was defined as migrating cell. Six randomly selected fields per membrane were imaged (Olympus IX73, Japan) and the number of the purple-stained cells was counted. The percentage of migrated cells was calculated using medium without serum in the bottom chamber as a reference. All experiments were repeated three times independently.

Statistical analysis

Results are expressed as means \pm the standard error of the mean (SEM). The data were analyzed by Student's *t*-test using Origin Statistic software (OriginLab Corporation, USA). A *p*-value < 0.05 was considered significant.

Results and Discussion

Electrochemical characterization of the assembled device

Our previous study demonstrated that MWCNT/graphene/MnO₂ specifically responds to H₂O₂. [41] To evaluate the stability of the sensor that immersed in cell culture medium for 24 h, 1 mM H₂O₂ was added into the medium at 0, 12, 18 and 24 h, and the CV response was recorded. The H₂O₂ induced peak current change (S1 Fig) shows that immersing the MWCNT/graphene/MnO₂ decorated electrode in cell culture medium for 24 h would not attenuate the function of the sensor. To realize H₂O₂ production *in situ*, attention has been paid on the amperometric response of the MWCNT/graphene/MnO₂ functionalized device to subsequent additions of H₂O₂ in cell culture medium (RPMI 1640). First, the choice of the applied potential at the working electrode is optimized to achieve a higher sensitivity. The amperometric *i-t* curves under potentials between -0.3 V and -0.5 V (*vs* ITO reference electrode/counter electrode, RE/CE) were recorded. As shown in supplementary S2 Fig, the best performance is obtained with a potential of -0.4 V *vs* ITO RE/CE. Therefore, the sensitivity of the device was monitored amperometrically at the working potential of -0.4 V *vs* ITO RE/CE. Deionized water (DI H₂O) and 4 μM H₂O₂ were subsequent added in medium. The amperometric response of adding DI water is barely observed; indicating the action of pipetting liquid into the reaction chamber does not spike noise (Fig 3A, curve *a*). While, the amperometric signal in curve *b* of Fig 3A shows that the device responds quickly to the change of H₂O₂ concentration. Inset of Fig 3A shows the calibration curve of the fully assembled device for H₂O₂ detection with a linear equation of Current (μA) = $-5.8 \times 10^{-4} - 0.00313 C_{\text{H}_2\text{O}_2}$ (H₂O₂ concentration, μM), of which the R² is 0.997 and standard error of the slope is 6.2×10^{-5} . The sensitivity of the fully assembled devices is 3.2 nAμM⁻¹cm⁻², based on the ratio of the slope of current-dose response curve and the surface area of electrode. Finally, human melanoma cells A375 (1 × 10⁵ cell) were cultured on the upper chamber of the device. The *in situ* monitoring of H₂O₂ release was investigated by using phorbol 12-myristate-13-acetate (PMA), a model drug known to trigger H₂O₂ production from human cells. Meanwhile, catalase, a H₂O₂ scavenger, was measured along with PMA to investigate the specificity of the *in situ* monitoring of H₂O₂ secreted from cells in the upper chamber. As presented in Fig 3B, no current response was observed from the device without cells (line: control 1) and the device with cultured cells under DMSO (solvent of PMA) injection (line: control 2). With the addition of catalase that can decompose H₂O₂ to water and oxygen, the reduction peak current increase caused by PMA injection decreases sharply (line: cell response). It has been reported that H₂O₂ can diffuse through cellular membranes to a distance even nearly 1mm because of its solubility in both lipid and aqueous environments and comparatively low reactivity. [33, 49] To investigate the effect of the cell location on H₂O₂ detection, we measured the production of H₂O₂ from cells growing in the upper and bottom PDMS chamber of the assembled device. A similar current intensity was observed from cells seeded in upper and bottom chamber upon PMA challenge (inset of Fig 3B), indicating the electrochemical sensor located at the bottom chamber can *in situ* sense H₂O₂ secreted from cells seeding in the top chamber.

Quantification of H₂O₂ generation during cell migration by electrochemical devices

Fig 2 lists experiment settings used in the migration assay with bi-module devices. In cell migration assay, serum-starved (8 h) melanoma A375 cells were studied as the model cell. Fetal bovine serum (FBS) was added to RPMI 1640 medium in the bottom chamber to establish nutrition chemo-attractant. Fig 4A shows the *in-situ* amperometric signal of the melanoma A375

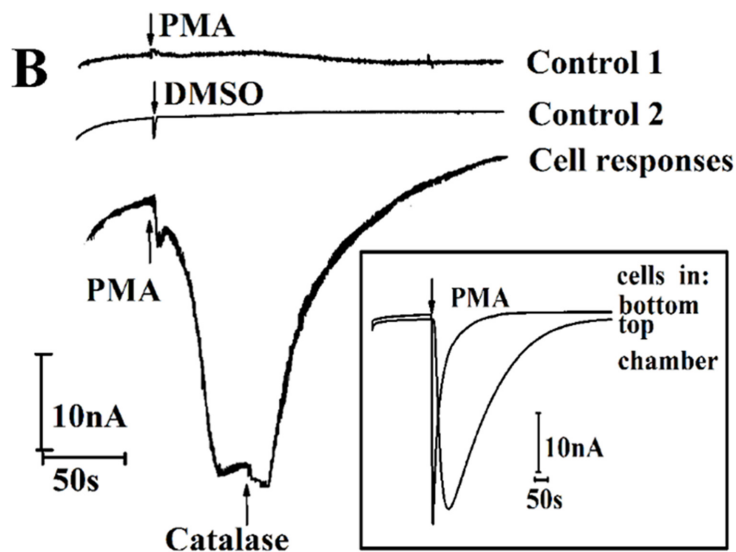
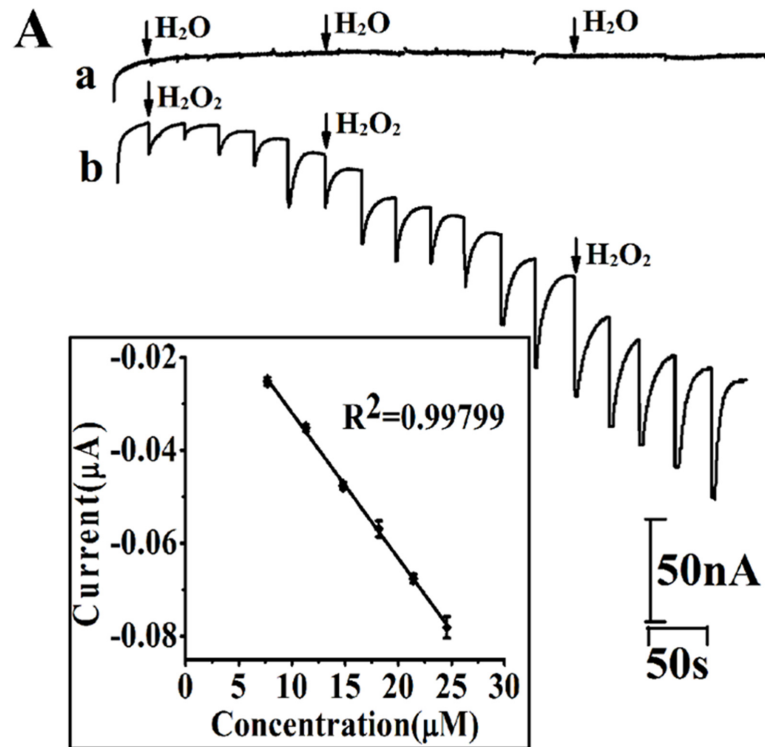


Fig 3. Amperometric performance (*i-t* curve) of fully assembled device. (A) *i-t* curves of successive additions of H₂O (a) or 4 μM H₂O₂ (b) into RPMI 1640 at an applied potential of -0.4 V vs ITO RE/CE; (B) *i-t* curves of PMA injection (0.5 mg mL⁻¹) without cells loading (control 1), DMSO (0.5%, v/v%) injection with cell loading (control 2), PMA injection (0.5 mg mL⁻¹) with cells loading, and followed by catalase injection (5 μg mL⁻¹)-cell response at an applied potential of -0.4 V vs ITO RE/CE; Inset of (B) *i-t* curves of PMA injection with cells loaded in top and bottom chamber of assembled device. RE/CE: reference electrode/ counter electrode; PMA: phorbol 12-myristate-13-acetate, DMSO: dimethyl sulfoxide

doi:10.1371/journal.pone.0127610.g003

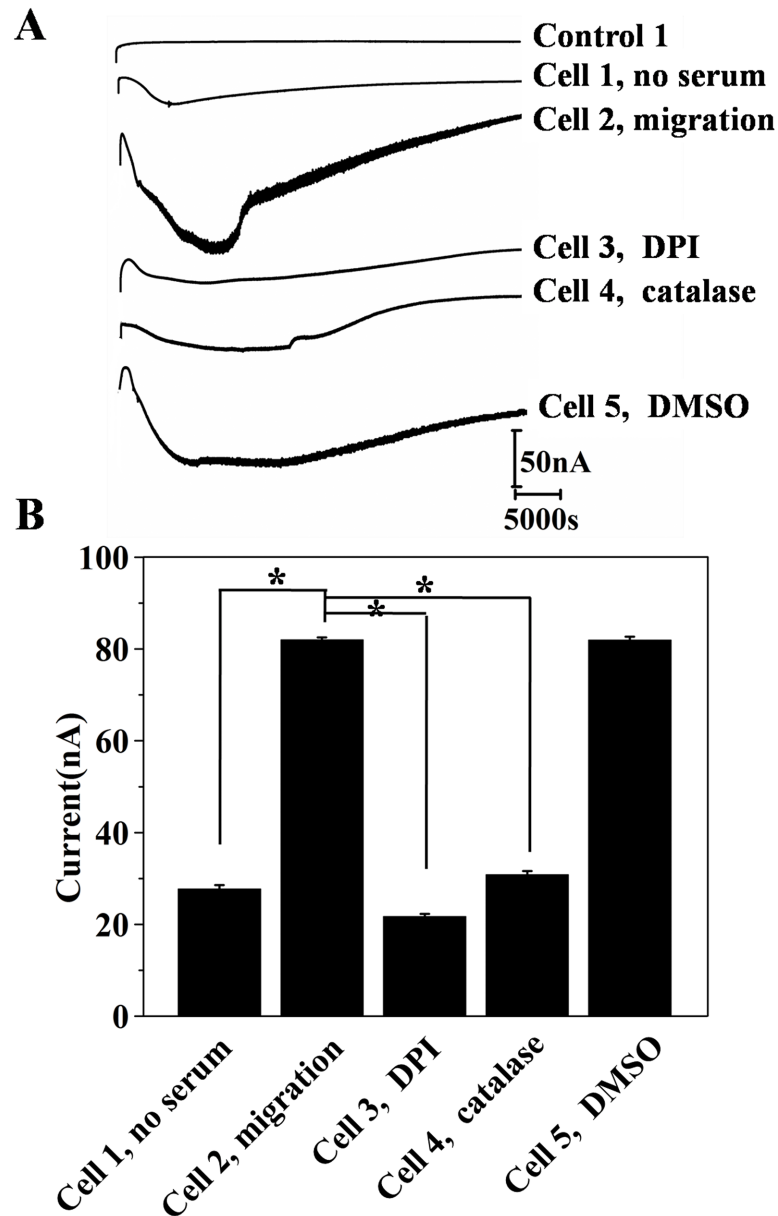


Fig 4. (A) Amperometric responses of fully functionalized bi-module device during melanoma A375 cell migration. *No cell*: device without cell loading; *No serum*: medium without serum in bottom chamber; *DPI*: RPMI 1640 containing 10% serum (conditioned medium) in bottom chamber, cell in upper chamber was incubated with H_2O_2 generation inhibitor, DPI; *Catalase*: conditioned medium in bottom chamber, cell in upper chamber was incubated with H_2O_2 decomposer, catalase; *Cell migration*: conditioned medium in bottom chamber; *DMSO*: conditioned medium in bottom chamber, cell in upper chamber was incubated with DMSO (solvent of DPI). (B) The corresponding current response obtained from amperometric curves of three independent experiments, ($n = 3$, * denotes $p < 0.05$). DPI: diphenyleneiodonium.

doi:10.1371/journal.pone.0127610.g004

cells that was monitored for 12 h at 37°C. The current baseline of the electrochemical device during a 12 h incubation time was recorded without cell loading (control 1). No visible current change was observed indicating the H_2O_2 will not automatically be generated from the medium during 12h incubation. The signal from cells that were seeded in a device with serum free medium in the bottom chamber was characterized as a migration control (cell 1, no serum in top

and bottom chamber). The amperometric track shows a current increase (16–28 nA) at the time course of 2–4 h, while the current gradually flows back during 5–7 h and stays stable during the rest of the assay time. We tested the H_2O_2 generated from cells seeded in a device in which RPMI 1640 medium plus 10% FBS (conditioned medium) was placed in the bottom chamber. The *in situ* measurement shows a cathode current increase trend and the current change reaches the maximum 84 ± 1 nA at 3h. For the rest of the time, the current gradually traced back to baseline (cell 2, migration). To specify that the amperometric signal was indeed given by H_2O_2 production during cell migration, NADH oxidase inhibitor DPI (10 μM) and H_2O_2 decomposer catalase (5 $\mu\text{g mL}^{-1}$) were used to pre-treat cells loaded in the upper chamber. Cell response 3 is the current signal from DPI pre-treated cells that were seeded in a device containing conditioned medium in the bottom chamber. A maximum current increase (23 ± 1 nA) can be read from the *i-t* curve. While, for cells incubated with catalase, a similar *i-t* curve was recorded. The impact of DMSO (solvent of DPI) on H_2O_2 production was measured in a cell migration section. Fig 4B shows the histogram of current change at a time point of 3h. The highest current change (84 ± 1 nA) is given by cells responding to medium containing 10% serum. The current value obtained from serum-starved cells incubated with DPI and catalase in devices that contained conditional medium (RPMI 1640 plus 10% FBS) in the bottom chamber are 23 ± 1 nA and 32 ± 2 nA, respectively, which are significantly lower than the non-pre-treated cells. Previous studies argued that DPI shows paradoxical effect in inducing DNA damage, mitochondria dysfunction and even apoptosis.[50–52] To investigate if the small current increase was caused by DPI impaired cell growth, we compared the viability of cells pre-treated by DPI, catalase and DMSO using MTT method (S3 Fig). The results show that DPI (10 μM) or catalase (5 $\mu\text{g mL}^{-1}$) does not reduce the viability of melanoma A375 cell.

In addition, according to the sensitivity of the electrochemical device as characterized in Fig 3A, H_2O_2 produced from cells can be calculated as detailed in the literature.[33, 41] At the 3h time point, the generated H_2O_2 from none pre-treated, DPI and catalase pre-treated cells are 0.13, 0.034 and 0.049 μM , respectively. Unlike previous fluorescent intensity qualitative descriptions of endogenous H_2O_2 variation, this is the first time that H_2O_2 production during a cell function has been directly quantified. According to the literature[21], exogenous 5 μM H_2O_2 enhances tumor cell migration. Thus, we investigated if endogenous H_2O_2 of one order lower level (0.1 μM) generated under chemotaxis would associate with the capability of cell migration.

To examine if the H_2O_2 production is associated with cell migration in the 12 h period, a migration experiment was conducted parallel to quantifying H_2O_2 with bi-module devices *in situ*. The polycarbonate membrane disassembled from the device was stained by hematoxylin and eosin (H&E) solution. Fig 5A shows the representative H&E staining images of polycarbonate membranes that was placed on a glass slide. The rod-like objects in all images are the micropore of the membrane. The migrating cells are characterized as purple-staining spot. More cells are observed from polycarbonate membrane that was disassembled from device containing serum-starved cell in the upper chamber and conditioned medium in the bottom chamber. Purple-staining cell sharply reduced on membrane from DPI and catalase pre-treatment groups. By counting the purple-staining cells from six random recorded microscopy images, the migration percentage was calculated using the group with no serum medium in bottom and top chamber as a reference. The results show that serum established chemotaxis induces $133 \pm 5\%$ and $143 \pm 6\%$ cell migration at 3, and 6 h (Fig 5B). Cells incubated with H_2O_2 generation inhibitor DPI can significantly reduce the chemotaxis triggered migration. The catalase pre-treated cells also show less migration ($-17 \pm 2\%$ and $14 \pm 2\%$ cell migrated at time of 3 and 6 h). Collectively, cell migration experiment on the bi-module device showed that serum-

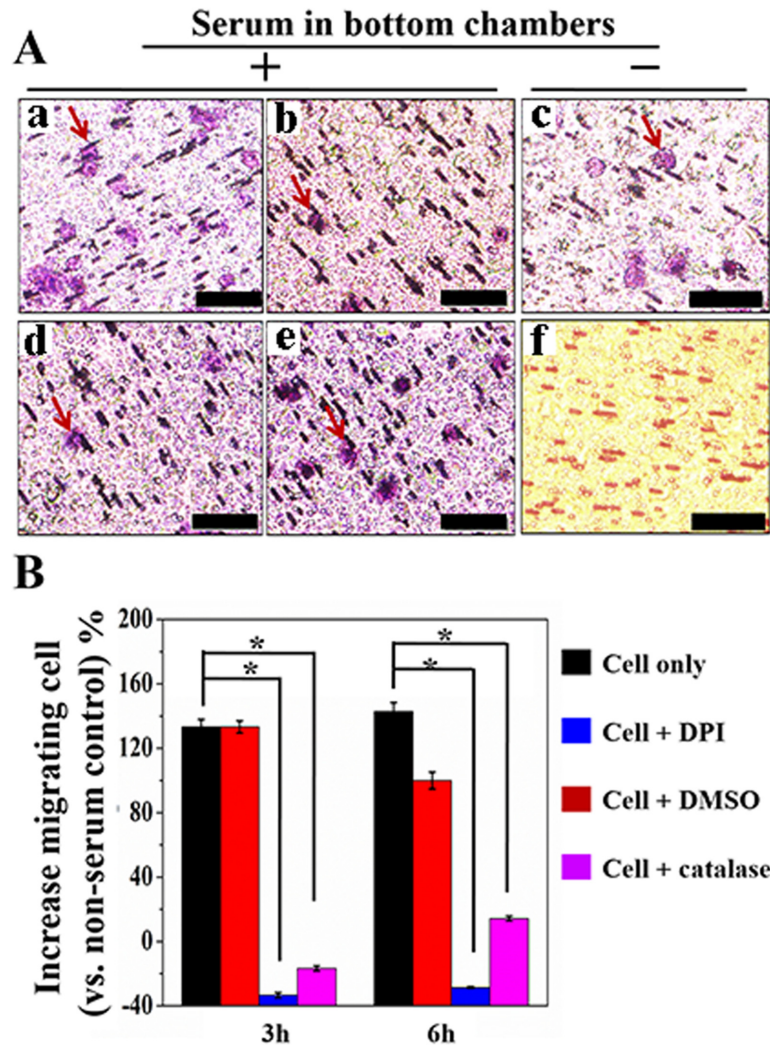


Fig 5. Cell migration quantified by hematoxylin and eosin (H&E) staining the polycarbonate membrane disassembled from device (A) photographs captured under microscopy: RPMI 1640 containing 10% serum in bottom chamber and serum-starved cells in top chamber (a), cells pre-treated by DPI (10 μ M) (b), cells pre-treated by catalase (5 μ g mL⁻¹) (d), cells pre-treated by DMSO (0.5%, V/V) (e), serum-starved cells in a device containing serum free medium in top and bottom chambers (c), and fresh polycarbonate membrane after (H&E) staining (f). Red arrow points the migrating cells. (B) histogram of migrating cell percentage using cells loaded in a device without serum in top and bottom chambers as a reference, * denotes $p < 0.01$, $n = 3$.

doi:10.1371/journal.pone.0127610.g005

starved cells under serum-established chemotaxis can produce H₂O₂, while the production of H₂O₂ is associated with cell motility.

Next, a Boyden chamber assay was conducted side-by-side to quantify cell migration. The results demonstrate that cells loaded with different cell densities can develop cell migration under serum-established chemotaxis (S4 Fig). Comparing with standard Boyden chamber assays, wound healing assay and previous reported on-chip cell migration platforms (Table 1), the bi-module device not only capable for study the morphology and functional changes of cells during cell migration, but monitor the generation of H₂O₂, an important reactive oxygen species having pathology and physiology significance.

Since cell motility is an important factor associated with tumor metastasis, we studied three types of tumor cells with bi-module devices. A375 cells are a well-recognized malignant

Table 1. Performance comparison of bi-module device with standard biological migration assay and lab-on-chip migration assay.

Assay platform	Morphology	Biochemical Molecule	Cell function	Chemotaxis	Ref
Bi-module device	YES	YES: Electrochemical analysis of H ₂ O ₂ generation during migration assay	YES: Migration of cells based on a serum established chemotaxis	YES	a
Boyden chamber	YES	NO	YES: Migration of cells into a wound to close the gap	YES	[20, 21]
Wound healing	YES	NO	YES: Migration of cells based on a chemical environment	NO	[19, 25]
On-chip ECIS	NO	NO	YES: Single cell migration	YES	[38]
On-chip wound healing	YES	NO	YES: Cell in responding to either promote or inhibit cell migration	YES	[42, 43]
Lab-on-Chip Mimicking cell surrounding	YES	NO	YES: 3D structure mimic micro-environment <i>in vivo</i> .	YES	[39, 41]
Assay platform	Morphology	Biochemical molecule	Cell function	Chemotaxis	Ref
Bi-module device	YES	YES: Electrochemical analysis of H ₂ O ₂ generation during migration assay	YES: Migration of cells based on a serum established chemotaxis	YES	a
Boyden chamber	YES	NO	YES: Migration of cells into a wound to close the gap	YES	[20, 21]
Wound healing	YES	NO	YES: Migration of cells based on a chemical environment	NO	[19, 25]
On-chip ECIS	NO	NO	YES: Single cell migration	YES	[38]
On-chip wound healing	YES	NO	YES: Cell in responding to either promote or inhibit cell migration	YES	[42, 43]
Lab-on-Chip Mimicking cell surrounding	YES	NO	YES: 3D structure mimic micro-environment <i>in vivo</i> .	YES	[39, 41]

a: this work;

H&E: hematoxylin and eosin; ECIS: electrical cell–substrate impedance sensing; 3D: three dimension

doi:10.1371/journal.pone.0127610.t001

melanoma cell line. The HEp-2 cell line was originated from tumors, which were produced in irradiated-cortisonised weanling rats after injection of epidermoid carcinoma tissue isolated from the larynx of a male. Hep G2 cells are a human liver carcinoma cell line and a suitable *in vitro* model system for the study of polarized human hepatocytes. Fig 6A presents typical amperometric signal traces of A375, HEp-2 and Hep G2 cells seeded in the upper chamber of bi-module device in which culture medium containing FBS was placed in the bottom chamber. The highest current value can be read at time point of 3.0, 4.0 and 1.5 h from the amperometric trace of A375, HEp-2 and Hep G2, respectively. And the maximum H₂O₂ production induced amperometric signal is 84±2 nA for A375 cells, 43±1 nA for HEp-2 cells and 39 ±1 nA for Hep G2 cells (Fig 6B) and the corresponding H₂O₂ concentration was 130±1.3 nM, 70±0.7 nM and 63±0.7 nM, respectively. The number of H₂O₂ molecule produced per cell is 6.5×10¹⁰, 3.6×10¹⁰ and 3.2×10¹⁰ for A375, HEp-2 and Hep G2 cell, respectively, calculating from the amperometric signal according to literatures.[33,41] Comparing to PMA triggered H₂O₂ production [33,41], the H₂O₂ molecule produced per cell under serum established chemotaxis is one order smaller. In a parallel experiment, we examined the migrating cells by counting the purple-staining cells on the polycarbonate membrane of the device. As shown in Fig 6C, more A375 cells can be observed from the H&E stained polycarbonate membrane. The average increased migrating cell of A375, HEp-2 and Hep G2 cells after 12 h incubation are 98±7%, 38±4% and 32±3%, respectively (Fig 6D). The quantitative analysis in Fig 6B and 6D confirms that a H₂O₂ production corresponds to cell motility.

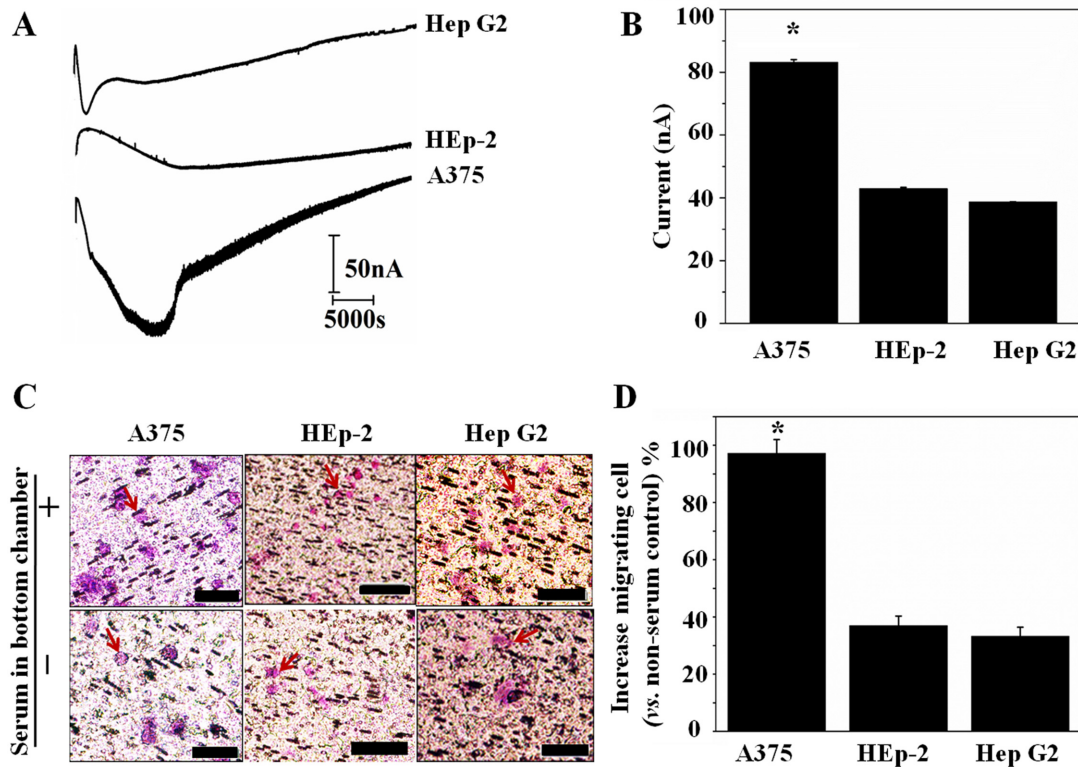


Fig 6. Cell migration quantified by bi-module device. (A) *in situ* amperometric signal of melanoma A375 cell, larynx HEp-2 cell and liver cancer Hep G2 cell seeded in device containing conditional medium (B) histogram of maximum current signal during 12h of cells; (C) H&E staining of migrating A375, Hep G2 and HEp-2 cells; (D) histogram of increased migrating cell percentage using cells loaded in a device without serum in bottom chamber as a reference, * denotes $p < 0.05$, $n = 3$.

doi:10.1371/journal.pone.0127610.g006

As characterized in supplementary S5 Fig, CV response of serum-starved cell in serum-free RPMI 1640 and RPMI 1640 are nearly identical. While adding of serum (10% FBS) into the serum-free medium leads to a reduction peak current increasing, indicating that serum would induce production of H_2O_2 from serum-starved cell. The phenomena is in line with documented information that growth factors can stimulate NADPH oxidase leading to the production of H_2O_2 . [53–55] The elevated endogenous H_2O_2 might trigger the activation of ERK and FAK signalling transduction pathways. The phosphorylation of ERK and FAK can lead to enhanced cell migration by activation downstream signalling proteins. [14, 53, 54] As illustrated in Fig 7, by using this device, for the first time, we quantified the H_2O_2 production in a trans-well cell migration setting. We anticipate the combination of electrochemical sensing with trans-well module can quantify other important biochemical molecules *in situ*, providing key information for depicting the relationship between biochemical signalling and cell function.

Conclusions

Hydrogen peroxide is believed to modulate signalling pathways that control cell motility. However, little is known about H_2O_2 generation during the cell migration process. A novel bi-module device was fabricated to characterize H_2O_2 production *in situ* while monitoring cell migration capability. For the first time, we quantified H_2O_2 molecule generation from cells

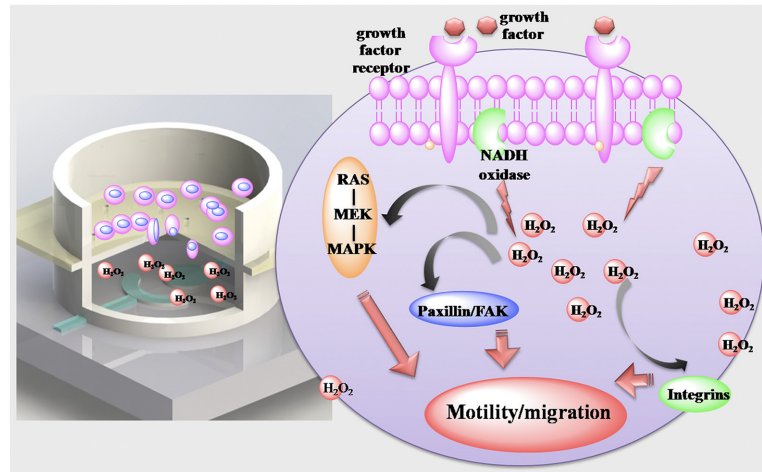


Fig 7. Bi-module device can *in situ* detects the generation of biochemical molecules in the process of cell migration.

doi:10.1371/journal.pone.0127610.g007

under a serum established chemotaxis is $\sim 6.5 \times 10^{10}$ per melanoma A375 cells, $\sim 3.6 \times 10^{10}$ per liver carcinoma Hep G2 cells and $\sim 3.2 \times 10^{10}$ per larynx carcinoma HEp-2 cells. In addition, a parallel migration assay with H_2O_2 generation inhibitor and decomposer demonstrated that the H_2O_2 generation is associated to cell migration. The bi-module cell migration platform enables *in situ* investigation for monitoring H_2O_2 production and cell function simultaneously, highlighting its potential for characterizing cell motility through monitoring cell secretion with rare samples and for investigation of mechanism of cell migration.

Supporting Information

S1 Fig. Cyclic voltammetric curves scanned at different time point. The electrochemical sensor was immersed in a cell culture medium for 24 h. At 0, 12, 18 and 24 h, $4 \mu M H_2O_2$ was added into the cell culture medium and the cyclic voltammetric (CV) curve was recorded. Then the increase of reduction peak current (Δ current) was compared. (TIF)

S2 Fig. Amperometric performance of electrode at different potential. The amperometric response of functionalized electrode at an applied potential of -0.3, -0.4, -0.45 and -0.5V vs ITO reference electrode/counter electrode (RE/CE) in responding to successive addition of $4 \mu M H_2O_2$ into RPMI 1640. (TIF)

S3 Fig. MTT cell growth assay. Melanoma A375 cells was seed in 96-well microplate (1×10^4 cell per well). DPI ($10 \mu M$), catalase ($5 \mu g mL^{-1}$) or DMSO (0.5%, V/V) were used to treat cells for 24 h. Then, $10 \mu L$ MTT solution was added to every well and incubated for 3 h. The purple-colored formazan products converted by viable cells were dissolved and measured using a spectrophotometric microplate reader (ELx800t, Gene Company) at 540 nm. The experiment was performed three independent times in triplicates. (TIF)

S4 Fig. Boyden chamber migration assay. Hematoxylin and eosin staining of migrating A375 examined in a Boyden chamber assay. Different concentration of cell suspensions was seed in the upper chamber and incubated for 24 h. The results were quantified using migrating cell

counted in an assay without serum in the bottom chamber as a reference. (TIF)

S5 Fig. H₂O₂ production from serum-starved cells by direct serum stimulation. Melanoma A375 cells were serum-starved for 8 h and then collected. RPMI 1640 medium was placed in the PDMS chamber and CV response was recorded. Then serum-starved cell (4×10^5) was pipetted into the chamber. After 10 min, the CV response was recorded. Finally, serum (10% FBS) was added into the chamber. The CV response was recorded after 30 min incubation. (TIF)

Acknowledgments

We thank Dr. Yuan Li (Chongqing Medical University) for providing cell line Hep G2 and HEP-2. This work is financially supported by Chongqing Key Laboratory for Advanced Materials and Technologies of Clean Energies, Start-up grant under SWU111071 from Southwest University, the National Science Foundation of China (No. 31200700,21375108), and Chongqing Key Natural Science Foundation (cstc2014jcyjA10070).

Author Contributions

Conceived and designed the experiments: LY YLT. Performed the experiments: YLT AXG. Analyzed the data: YLT ZZZ. Contributed reagents/materials/analysis tools: LY YLT CML. Wrote the paper: LY YSL. Obtained permission for use of cell line: LZ.

References

1. Lauffenburger DA, Horwitz AF. (1996) Cell migration: a physically integrated molecular process. *Cell*. 84(3):359–69. PMID: [8608589](#)
2. Lauffenburger DA. Cell motility. (1996) Making connections count. *Nature*. 383(6599):390–1. PMID: [8837766](#)
3. Stroka KM, Konstantopoulos K. (2014) Physical biology in cancer. 4. Physical cues guide tumor cell adhesion and migration. *Am J Physiol Cell Physiol*. 306(2):C98–C109. doi: [10.1152/ajpcell.00289.2013](#) PMID: [24133064](#)
4. Bravo-Cordero JJ, Magalhaes MA, Eddy RJ, Hodgson L, Condeelis J. (2013) Functions of cofilin in cell locomotion and invasion. *Nat Rev Mol Cell Biol*. 14(7):405–15. doi: [10.1038/nrm3609](#) PMID: [23778968](#)
5. Bouvard D, Pouwels J, De Franceschi N, Ivaska J. (2013) Integrin inactivators: balancing cellular functions in vitro and in vivo. *Nat Rev Mol Cell Biol*. 14(7):430–42. doi: [10.1038/nrm3599](#) PMID: [23719537](#)
6. Schwartz MA, Horwitz AR. Integrating adhesion, protrusion, and contraction during cell migration. (2006) *Cell*. 125(7):1223–5. PMID: [16814706](#)
7. Kohn EC, Liotta LA. (1993) Invasion and metastasis: new approaches to an old problem. *Oncology (Williston Park)*. 7(4):47–52. PMID: [8485035](#)
8. Entschladen F, Drell TL, Lang K, Joseph J, Zaenker KS. (2004) Tumour-cell migration, invasion, and metastasis: navigation by neurotransmitters. *Lancet Oncol*. 5(4):254–8. PMID: [15050959](#)
9. Polacheck WJ, Zervantonakis IK, Kamm RD. (2013) Tumor cell migration in complex microenvironments. *Cell Mol Life Sci*. 70(8):1335–56. doi: [10.1007/s00018-012-1115-1](#) PMID: [22926411](#)
10. Dinic J, Ashrafzadeh P, Parmryd I. (2013) Actin filaments attachment at the plasma membrane in live cells cause the formation of ordered lipid domains. *Biochim Biophys Acta*. 1828(3):1102–11. doi: [10.1016/j.bbame.2012.12.004](#) PMID: [23246974](#)
11. Jiang Q, Zhou C, Bi Z, Wan Y. (2006) EGF-induced cell migration is mediated by ERK and PI3K/AKT pathways in cultured human lens epithelial cells. *J Ocul Pharmacol Ther*. 22(2):93–102. PMID: [16722795](#)
12. Chen H, Zhu G, Li Y, Padia RN, Dong Z, Pan ZK, et al. (2009) Extracellular signal-regulated kinase signaling pathway regulates breast cancer cell migration by maintaining slug expression. *Cancer Res* 69(24):9228–35. doi: [10.1158/0008-5472.CAN-09-1950](#) PMID: [19920183](#)

13. Chen YJ, Tsai RK, Wu WC, He MS, Kao YH, Wu WS. (2012) Enhanced PKC δ and ERK signaling mediate cell migration of retinal pigment epithelial cells synergistically induced by HGF and EGF. *PLoS one*. 7(9):e44937. doi: [10.1371/journal.pone.0044937](https://doi.org/10.1371/journal.pone.0044937) PMID: [23028692](https://pubmed.ncbi.nlm.nih.gov/23028692/)
14. Liu LZ, Hu XW, Xia C, He J, Zhou Q, Shi X, et al. (2006) Reactive oxygen species regulate epidermal growth factor-induced vascular endothelial growth factor and hypoxia-inducible factor-1 α expression through activation of AKT and P70S6K1 in human ovarian cancer cells. *Free Radic Biol Med*. 41(10):1521–33. PMID: [17045920](https://pubmed.ncbi.nlm.nih.gov/17045920/)
15. Lee DJ, Kang SW. (2013) Reactive oxygen species and tumor metastasis. *Mol Cells*. 35(2):93–8. doi: [10.1007/s10059-013-0034-9](https://doi.org/10.1007/s10059-013-0034-9) PMID: [23456330](https://pubmed.ncbi.nlm.nih.gov/23456330/)
16. Usatyuk PV, Fu P, Mohan V, Epshtein Y, Jacobson JR, Gomez-Cambronero J, et al. (2014) Role of c-Met/PI3K/Akt Signaling in HGF-mediated Lamellipodia Formation, ROS Generation and Motility of Lung Endothelial Cells. *J Biol Chem*. 289(19):13476–91. doi: [10.1074/jbc.M113.527556](https://doi.org/10.1074/jbc.M113.527556) PMID: [24634221](https://pubmed.ncbi.nlm.nih.gov/24634221/)
17. Hung WY, Huang KH, Wu CW, Chi CW, Kao HL, Li AF, et al. (2012) Mitochondrial dysfunction promotes cell migration via reactive oxygen species-enhanced β 5-integrin expression in human gastric cancer SC-M1 cells. *Biochim Biophys Acta*. 1820(7):1102–10. doi: [10.1016/j.bbagen.2012.04.016](https://doi.org/10.1016/j.bbagen.2012.04.016) PMID: [22561002](https://pubmed.ncbi.nlm.nih.gov/22561002/)
18. Wang Y, Zang QS, Liu Z, Wu Q, Maass D, Dulán G, et al. (2011) Regulation of VEGF-induced endothelial cell migration by mitochondrial reactive oxygen species. *Am J Physiol Cell Physiol*. 301(3):C695–704. doi: [10.1152/ajpcell.00322.2010](https://doi.org/10.1152/ajpcell.00322.2010) PMID: [21653897](https://pubmed.ncbi.nlm.nih.gov/21653897/)
19. Im YS, Ryu YK, Moon EY. (2012) Mouse Melanoma Cell Migration is Dependent on Production of Reactive Oxygen Species under Normoxia Condition. *Biomol Ther*. 20(2):165–70. doi: [10.4062/biomolther.2012.20.2.165](https://doi.org/10.4062/biomolther.2012.20.2.165) PMID: [24116290](https://pubmed.ncbi.nlm.nih.gov/24116290/)
20. Tobar N, Guerrero J, Smith PC, Martinez J. (2010) NOX4-dependent ROS production by stromal mammary cells modulates epithelial MCF-7 cell migration. *Br J Cancer*. 103(7):1040–7. doi: [10.1038/sj.bjc.6605847](https://doi.org/10.1038/sj.bjc.6605847) PMID: [20717118](https://pubmed.ncbi.nlm.nih.gov/20717118/)
21. Polytaichou C, HatziaPOSTOLOU M, Papadimitriou E. (2005) Hydrogen peroxide stimulates proliferation and migration of human prostate cancer cells through activation of activator protein-1 and up-regulation of the heparin affinity regulatory peptide gene. *J Biol Chem*. 280(49):40428–35. PMID: [16199533](https://pubmed.ncbi.nlm.nih.gov/16199533/)
22. Luanpitpong S, Talbott SJ, Rojanasakul Y, Nimmannit U, Pongrakhananon V, Wang L, et al. (2010) Regulation of lung cancer cell migration and invasion by reactive oxygen species and caveolin-1. *J Biol Chem*. 285(50):38832–40. doi: [10.1074/jbc.M110.124958](https://doi.org/10.1074/jbc.M110.124958) PMID: [20923773](https://pubmed.ncbi.nlm.nih.gov/20923773/)
23. DeGennaro M, Hurd TR, Siekhaus DE, Biteau B, Jasper H, Lehmann R. (2011) Peroxiredoxin stabilization of DE-cadherin promotes primordial germ cell adhesion. *Dev Cell*. 20(2):233–43. doi: [10.1016/j.devcel.2010.12.007](https://doi.org/10.1016/j.devcel.2010.12.007) PMID: [21316590](https://pubmed.ncbi.nlm.nih.gov/21316590/)
24. Wu WS, Tsai RK, Chang CH, Wang S, Wu JR, Chang YX. (2006) Reactive oxygen species mediated sustained activation of protein kinase C α and extracellular signal-regulated kinase for migration of human hepatoma cell Hep G2. *Mol Cancer Res*. 4(10):747–58. PMID: [17050668](https://pubmed.ncbi.nlm.nih.gov/17050668/)
25. Basuroy S, Dunagan M, Sheth P, Seth A, Rao RK. (2010) Hydrogen peroxide activates focal adhesion kinase and c-Src by a phosphatidylinositol 3 kinase-dependent mechanism and promotes cell migration in Caco-2 cell monolayers. *Am J Physiol Gastrointest Liver Physiol*. 299(1):G186–95. doi: [10.1152/ajpgi.00368.2009](https://doi.org/10.1152/ajpgi.00368.2009) PMID: [20378826](https://pubmed.ncbi.nlm.nih.gov/20378826/)
26. Pan Q, Qiu WY, Huo YN, Yao YF, Lou MF. (2011) Low levels of hydrogen peroxide stimulate corneal epithelial cell adhesion, migration, and wound healing. *Invest Ophthalmol Vis Sci*. 52(3):1723–34. doi: [10.1167/iovs.10-5866](https://doi.org/10.1167/iovs.10-5866) PMID: [21087961](https://pubmed.ncbi.nlm.nih.gov/21087961/)
27. Sadok A, Bourgarel-Rey V, Gattacceca F, Penel C, Lehmann M, Kovacic H. (2008) Nox1-dependent superoxide production controls colon adenocarcinoma cell migration. *Biochim Biophys Acta*. 1783(1):23–33. PMID: [18023288](https://pubmed.ncbi.nlm.nih.gov/18023288/)
28. Lee ER, Kim JH, Kang YJ, Cho SG. (2007) The anti-apoptotic and anti-oxidant effect of eriodictyol on UV-induced apoptosis in keratinocytes. *Biol Pharm Bull*. 30(1):32–7. PMID: [17202655](https://pubmed.ncbi.nlm.nih.gov/17202655/)
29. Peus D, Vasa RA, Meves A, Pott M, Beyerle A, Squillace K, et al. (1998) H₂O₂ is an important mediator of UVB-induced EGF-receptor phosphorylation in cultured keratinocytes. *J Invest Dermatol*. 110(6):966–71. PMID: [9620307](https://pubmed.ncbi.nlm.nih.gov/9620307/)
30. Achyuta AK, Stephens KD, Lewis HG, Murthy SK. (2010) Mitigation of reactive human cell adhesion on poly(dimethylsiloxane) by immobilized trypsin. *Langmuir*. 26(6):4160–7. doi: [10.1021/la903441u](https://doi.org/10.1021/la903441u) PMID: [20214394](https://pubmed.ncbi.nlm.nih.gov/20214394/)
31. Winterbourn CC. (2014) The challenges of using fluorescent probes to detect and quantify specific reactive oxygen species in living cells. *Biochim Biophys Acta*. 1840(2):730–8. doi: [10.1016/j.bbagen.2013.05.004](https://doi.org/10.1016/j.bbagen.2013.05.004) PMID: [23665586](https://pubmed.ncbi.nlm.nih.gov/23665586/)

32. Grisham MB. (2013) Methods to detect hydrogen peroxide in living cells: Possibilities and pitfalls. *Comp Biochem Physiol A Mol Integr Physiol.* 165(4):429–38. doi: [10.1016/j.cbpa.2013.02.003](https://doi.org/10.1016/j.cbpa.2013.02.003) PMID: [23396306](https://pubmed.ncbi.nlm.nih.gov/23396306/)
33. Guo CX, Zheng XT, Lu ZS, Lou XW, Li CM. (2010) Biointerface by cell growth on layered graphene-artificial peroxidase-protein nanostructure for in situ quantitative molecular detection. *Adv Mater.* 22(45):5164–7. doi: [10.1002/adma.201001699](https://doi.org/10.1002/adma.201001699) PMID: [20878626](https://pubmed.ncbi.nlm.nih.gov/20878626/)
34. Lahdesmaki I, Park YK, Carroll AD, Decuir M, Ruzicka J. (2007) In-situ monitoring of H₂O₂ degradation by live cells using voltammetric detection in a lab-on-valve system. *Analyst.* 132(8):811–7. PMID: [17646881](https://pubmed.ncbi.nlm.nih.gov/17646881/)
35. Manning P, McNeil CJ. (2011) Electrochemical and optical sensing of reactive oxygen species: pathway to an integrated intracellular and extracellular measurement platform. *Biochem Soc Trans.* 39(5):1288–92. doi: [10.1042/BST0391288](https://doi.org/10.1042/BST0391288) PMID: [21936803](https://pubmed.ncbi.nlm.nih.gov/21936803/)
36. Yu L, Gao LX, Ma XQ, Hu FX, Shi ZZ, Li CM, Lu ZS. (2014) Involvement of Superoxide and Nitric Oxide in BRAFV600E Inhibitor PLX4032-induced Cell Growth Inhibition of Melanoma Cells. *Integr Biol-UK.* 6(12): 1211–1217 doi: [10.1039/c4ib00170b](https://doi.org/10.1039/c4ib00170b) PMID: [25363644](https://pubmed.ncbi.nlm.nih.gov/25363644/)
37. Rabinowitz JD, Vacchino JF, Beeson C, McConnell HM. (1998) Potentiometric Measurement of Intracellular Redox Activity. *J Am Chem Soc.* 120: 2464–2473
38. Eklund SE, Snider RM, Wikswo J, Baudenbacher F, Prokop A, Cliffel DE. (2006) Multianalyte microphysiometry as a tool in metabolomics and systems biology. *J Electroanal Chem.* 587(2):333–339
39. Eklund SE, Cliffel DE, Kozlov E, Prokop A, Wikswo J, Baudenbacher F. (2003) Modification of Cytosensor™ microphysiometer to simultaneously measure extracellular acidification and oxygen consumption rates. *Anal Chim Acta.* 496(1–2): 93–101
40. Snider RM, Ciobanu M, Rue AE, Cliffel DE. (2008) A multiwalled carbon nanotube/dihydropyran composite film electrode for insulin detection in a microphysiometer chamber. *Anal Chim Acta.* 609(1): 44–52 doi: [10.1016/j.aca.2007.12.032](https://doi.org/10.1016/j.aca.2007.12.032) PMID: [18243872](https://pubmed.ncbi.nlm.nih.gov/18243872/)
41. Shi ZZ, Wu XS, Gao LX, Tian YL, Yu L. (2014) Electrodes/paper sandwich devices for in situ sensing of hydrogen peroxide secretion from cells growing in gels-in-paper 3 dimensional matrix. *Anal Meth.* 6(12):4446–54.
42. Nguyen TA, Yin TI, Reyes D, Urban GA. (2013) Microfluidic chip with integrated electrical cell-impedance sensing for monitoring single cancer cell migration in three-dimensional matrixes. *Anal Chem.* 85(22):11068–76. doi: [10.1021/ac402761s](https://doi.org/10.1021/ac402761s) PMID: [24117341](https://pubmed.ncbi.nlm.nih.gov/24117341/)
43. Zervantonakis IK, Hughes-Alford SK, Charest JL, Condeelis JS, Gertler FB, Kamm RD. (2012) Three-dimensional microfluidic model for tumor cell intravasation and endothelial barrier function. *Proc Natl Acad Sci U S A.* 109(34):13515–20. doi: [10.1073/pnas.1210182109](https://doi.org/10.1073/pnas.1210182109) PMID: [22869695](https://pubmed.ncbi.nlm.nih.gov/22869695/)
44. Li J, Lin F. (2011) Microfluidic devices for studying chemotaxis and electrotaxis. *Trends Cell Biol.* 21(8):489–97. doi: [10.1016/j.tcb.2011.05.002](https://doi.org/10.1016/j.tcb.2011.05.002) PMID: [21665472](https://pubmed.ncbi.nlm.nih.gov/21665472/)
45. Jeong GS, Kwon GH, Kang AR, Jung BY, Park Y, Chung S, et al. (2011) Microfluidic assay of endothelial cell migration in 3D interpenetrating polymer semi-network HA-Collagen hydrogel. *Biomed Microdevices.* 13(4):717–23. doi: [10.1007/s10544-011-9541-7](https://doi.org/10.1007/s10544-011-9541-7) PMID: [21494794](https://pubmed.ncbi.nlm.nih.gov/21494794/)
46. van der Meer AD, Vermeul K, Poot AA, Feijen J, Vermes I. (2010) A microfluidic wound-healing assay for quantifying endothelial cell migration. *Am J Physiol Heart Circ Physiol.* 298(2):H719–25. doi: [10.1152/ajpheart.00933.2009](https://doi.org/10.1152/ajpheart.00933.2009) PMID: [19933413](https://pubmed.ncbi.nlm.nih.gov/19933413/)
47. Nie FQ, Yamada M, Kobayashi J, Yamato M, Kikuchi A, Okano T. (2007) On-chip cell migration assay using microfluidic channels. *Biomaterials.* 28(27):4017–22. PMID: [17583787](https://pubmed.ncbi.nlm.nih.gov/17583787/)
48. Wang X, Osada T, Wang Y, Yu L, Sakakura K, Katayama A, et al. (2010) CSPG4 protein as a new target for the antibody-based immunotherapy of triple-negative breast cancer. *J Natl Cancer Inst.* 102(19): 1496–1512 doi: [10.1093/jnci/djq343](https://doi.org/10.1093/jnci/djq343) PMID: [20852124](https://pubmed.ncbi.nlm.nih.gov/20852124/)
49. Park WH. (2013) The effects of exogenous H₂O₂ on cell death, reactive oxygen species and glutathione levels in calf pulmonary artery and human umbilical vein endothelial cells. *Int J Mol Med.* 31(2):471–6. doi: [10.3892/ijmm.2012.1215](https://doi.org/10.3892/ijmm.2012.1215) PMID: [23254439](https://pubmed.ncbi.nlm.nih.gov/23254439/)
50. Park SE, Song JD, Kim KM, Park YM, Kim ND, Yoo YH, et al. (2007) Diphenyleiiodonium induces ROS-independent p53 expression and apoptosis in human RPE cells. *FEBS Lett.* 581(2):180–6. PMID: [17184774](https://pubmed.ncbi.nlm.nih.gov/17184774/)
51. Li N, Ragheb K, Lawler G, Sturgis J, Rajwa B, Melendez JA, et al. (2003) DPI induces mitochondrial superoxide-mediated apoptosis. *Free Radic Biol Med.* 34(4): 465–77. PMID: [12566072](https://pubmed.ncbi.nlm.nih.gov/12566072/)
52. Longpre JM, Loo G. (2008) Paradoxical effect of diphenyleiiodonium in inducing DNA damage and apoptosis. *Free Radic Res.* 42(6): 533–43. doi: [10.1080/10715760802126692](https://doi.org/10.1080/10715760802126692) PMID: [18569011](https://pubmed.ncbi.nlm.nih.gov/18569011/)

53. Bae YS, Sung JY, Kim OS, Kim YJ, Hur KC, Kazlauskas A, et al. (2000) Platelet-derived growth factor-induced H₂O₂ production requires the activation of phosphatidylinositol 3-kinase. *J. Biol. Chem.* 275(14):10527–31. PMID: [10744745](#)
54. Bae YS, Kang SW, Seo MS, Baines IC, Tekle E, Chock PB, et al. (1997) Epidermal growth factor (EGF)-induced generation of hydrogen peroxide. Role in EGF receptor-mediated tyrosine phosphorylation. *J. Biol. Chem.* 272(1):217–21. PMID: [8995250](#)
55. Hu T, Ramachandrarao SP, Siva S, Valancius C, Zhu Y, Mahadev K, et al. (2005) Reactive oxygen species production via NADPH oxidase mediates TGF-beta-induced cytoskeletal alterations in endothelial cells. *Am J Physiol Renal Physiol* 289(4):F816–25. PMID: [16159901](#)